Scientific Research Publishing

International Journal of Astronomy and Astrophysics, 2025, 15(4), 336-355
https://www.scirp.org/journal/ijaa
ISSN Online: 2161-4725
ISSN Print: 2161-4717

Warm Dark Matter Studies with Spiral Galaxy Data

Bruce Hoeneisen

Universidad San Francisco de Quito, Quito, Ecuador
Email: bhoeneisen@usfq.edu.ec

How to cite this paper: Hoeneisen, B. (2025) Warm Dark Matter Studies with Spiral Galaxy Data. *International Journal of Astronomy and Astrophysics*, **15**, 336-355.
https://doi.org/10.4236/ijaa.2025.154021

Received: September 11, 2025
Accepted: November 1, 2025
Published: November 4, 2025

Copyright © 2025 by author(s) and Scientific Research Publishing Inc.
This work is licensed under the Creative Commons Attribution International License (CC BY 4.0).
http://creativecommons.org/licenses/by/4.0/

Open Access

Abstract

We measure the "warmness" of the dark matter, *i.e.* the comoving root-mean-square thermal velocity $v_{hrms}(1)$, with nearly 3000 spiral galaxy rotation curves in the PROBES catalog. The results are $v_{hrms}(1) = 700 \pm 165$ m/s if dark matter is collisional, or $v_{hrms}(1) \approx 280 \pm 95$ m/s if dark matter is collisionless. These results are in agreement with previous measurements of $v_{hrms}(1)$, and with independent measurements of the linear density power spectrum cut-off wavevector k_{fs} due to free-streaming, but are in disagreement with limits. This disagreement is not currently understood.

Keywords

Warm Dark Matter, Spiral Galaxies

1. Introduction

Most matter in the universe is in a "dark matter" form that has only been observed through its gravitational interaction. In the ΛCDM cosmology model it is assumed that dark matter is cold, *i.e.* is a gas of particles with negligible thermal velocity to affect galaxy formation. Cold dark matter is in agreement with large scale observations, but runs into several tensions at small scales, notably the galaxy core-cusp problem. Cold dark matter simulations obtain galaxy cusps, while observations often obtain cores. One alternative to cold dark matter is warm dark matter, either collisionless or collisional. The "warmness" of dark matter can be measured by studying the density runs of galaxy cores. These density runs can be measured with galaxy rotation curves, strong gravitational lensing, or by measuring stellar velocities. An alternative way to study warm dark matter is to observe the consequences of "free-streaming": the motion of dark matter particles erases small scale

density fluctuations suppressing the number densities of small galaxies. It turns out that these two approaches, cores and free-streaming, obtain results that are in disagreement with each other, and this disagreement is not currently understood.

In the present work we try to measure the "warmness" of dark matter studying the cores of nearly 3000 spiral galaxies with data in the *Photometry and Rotation Curve Observations from Extragalactic Surveys* (PROBES) catalog [1]. This data includes rotation curves obtained from long slit Hα spectra and HI (21 cm) velocity maps, combined with photometry of GALEX, DESI-LIS, and WISE images.

The following sections describe the theoretical framework, the data set, studies of this data, a discussion of how the thermal velocity is extracted from this data, a comparison with previous measurements, a comment on the discrepancy between measurements and limits, a comment on collisional *vs* collisionless dark matter, and conclusions.

2. The Theoretical framework

We measure the warm dark matter adiabatic invariant

$$v_{h\mathrm{rms}}(1) \equiv v_{h\mathrm{rms}}(a)a = v_{h\mathrm{rms}}(a)\left(\frac{\Omega_c\rho_{\mathrm{crit}}}{\rho_h(a)}\right)^{1/3} \tag{1}$$

with data of nearly 3000 spiral galaxies in the PROBES catalog [1]. We assume dark matter is a gas of particles of mass m_h. These particles are assumed to be collisionless, or have dark matter-dark matter elastic collisions, but otherwise only have gravitational interactions. $a(t)$ is the expansion parameter of the universe, normalized to $a(t_0)=1$ at the present time t_0. $v_{h\mathrm{rms}}(a)$ is the root-mean-square of the non-relativistic warm dark matter particle thermal velocities, and $\rho_h(a)$ is the warm dark matter density, when the early universe is nearly homogeneous at $a \ll 1$. $v_{h\mathrm{rms}}(a)$ scales as a^{-1} [2] and $\rho_h(a)$ is proportional to a^{-3}, so the comoving thermal velocity $v_{h\mathrm{rms}}(1)$ is an adiabatic invariant: it defines the "warmness" of dark matter.

We use the standard notation in cosmology as defined in [3], and the parameter values therein. For example, $\Omega_c\rho_{\mathrm{crit}}$ is the present day mean dark matter density. We use the sub-indices h and b to denote the dark matter halo and "baryons" respectively (in cosmology, "baryons" generally refer to all non-relativistic matter, excluding dark matter and neutrinos).

Imagine an observer in a density peak in the early universe. This observer feels no gravity and "sees" dark matter expand and then contract into the core of a galaxy. If this expansion and contraction were adiabatic we could extract the adiabatic invariant $v_{h\mathrm{rms}}(1)$ from two galaxy observables: the root-mean-square of the radial thermal velocity of the dark matter particles $\sqrt{\langle v_{rh}^2\rangle}$ and the galaxy core dark matter density ρ_{ch}:

$$v'_{h\mathrm{rms}}(1) \equiv \sqrt{3}\sqrt{\langle v_{rh}^2\rangle}\left(\frac{\Omega_c\rho_{\mathrm{crit}}}{\rho_{ch}}\right)^{1/3}. \tag{2}$$

Note that if dark matter is an ideal noble gas, *i.e.* has elastic dark matter-dark matter collisions (that do not excite the particles), then the velocity distribution of the dark matter particles is the Maxwell distribution, $\frac{1}{2}m_h\left\langle v_h^2\right\rangle=\frac{3}{2}kT$, and $TV^{\gamma-1}$ with $\gamma=5/3$ remains constant in an adiabatic expansion, which is equivalent to $v'_{h\mathrm{rms}}(1)$ constant. Here T and V are temperature and volume. If dark matter is collisionless, there is a geometrical factor f to be presented below.

From studies of baryon and total (dark matter plus baryon) spiral galaxy rotation curves, we describe the galaxy as two self-gravitating gases, dark matter and baryons, separately in thermal equilibrium (the fits obtain different temperatures so we neglect dark matter-baryon interactions). The densities $\rho_h(r)$ and $\rho_b(r)$ are obtained by integrating numerically hydrostatic equations [4] [5].

The PROBES galaxies generally have $\rho_{ch}>\rho_{cb}$, so we will treat baryons as a correction, see **Figure 1**. In this case the solution to the hydrostatic equations is the cored isothermal sphere. Let us recall that a cored isothermal sphere is defined by two parameters: the central dark matter density ρ_{ch}, and the root-mean-square of the radial thermal velocity $\sqrt{\left\langle v_{rh}^2\right\rangle}$ that is independent of the radial coordinate r. At large r the dark matter density is

$$\rho_h(r)=\frac{\left\langle v_{rh}^2\right\rangle}{2\pi Gr^2},\ \text{for } r\gg r_c. \tag{3}$$

The core radius is defined as

$$r_c\equiv\sqrt{\frac{\left\langle v_{rh}^2\right\rangle}{2\pi G\rho_{ch}}}. \tag{4}$$

Let $V(r)$ be the velocity of rotation of a test particle. At $r\gg r_c$, $V(r)=V_{\max}=\sqrt{2\left\langle v_{rh}^2\right\rangle}$ is independent of r (in the cored isothermal approximation). At a small $r_{\min}\ll r_c$ the derivative of the rotation velocity determines the core density:

$$\rho_{ch}=\left(\frac{V(r_{\min})}{r_{\min}}\right)^2\frac{3f_M}{4\pi G}, \tag{5}$$

where

$$f_M=\frac{M_{\mathrm{dyn}}(r_{\min})-M_*(r_{\min})}{M_{\mathrm{dyn}}(r_{\min})} \tag{6}$$

is the correction factor shown in **Figure 1**. $M_{\mathrm{dyn}}(r_{\min})$ is the total (dark matter plus baryon) mass within $r_{\min}$ (obtained from the rotation curves), and $M_*(r_{\min})$ is the corresponding stellar mass (obtained from multy-filter stellar mass synthesis models). We neglect the mass of gas and dust. For this correction, we choose $r_{\min}$ so 25% of the dynamical mass comes from within $r_{\min}$.

To summarize, our studies will focus on two spiral galaxy observables: $V(r_{\min})/r_{\min}$ and $V_{\max}$. From these two observables we obtain ρ_{ch}, r_c and $v'_{h\mathrm{rms}}(1)$. The relation between $v'_{h\mathrm{rms}}(1)$ and $v_{h\mathrm{rms}}(1)$ is

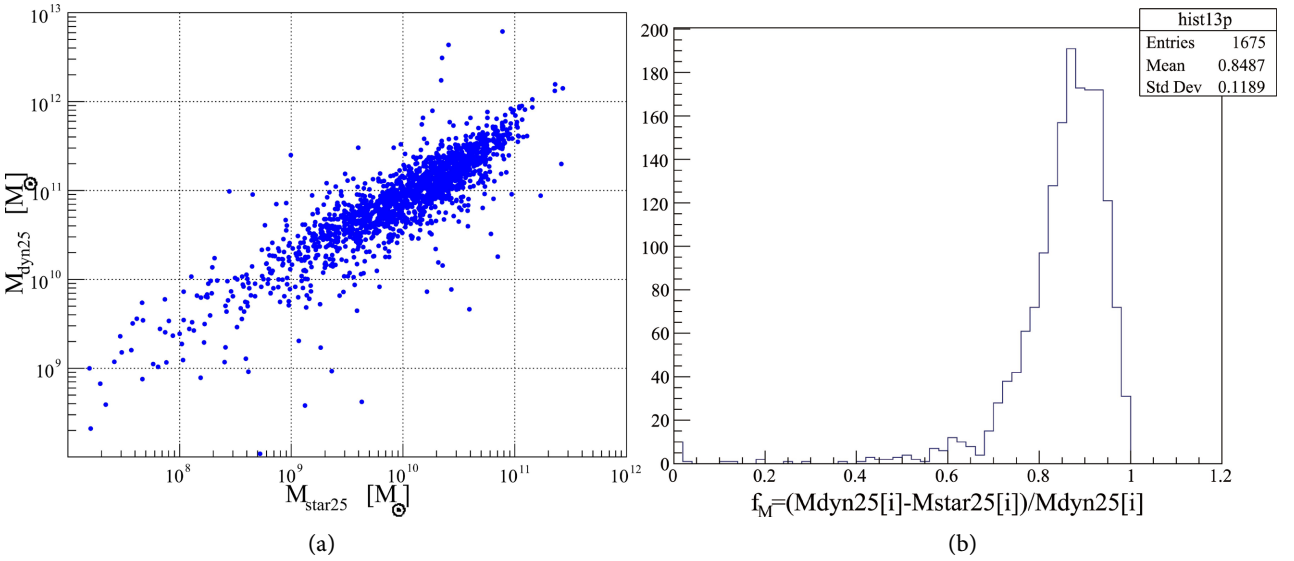

Figure 1. Left: Distribution of galaxy stellar mass M_* and dynamical (total dark matter plus baryon) mass $M_{\rm dyn}$ within a radius r_{25} containing 25% of the dynamical mass. Right: Correction factor $f_M = \left(M_{\rm dyn} - M_*\right)/M_{\rm dyn}$. All data in this article is obtained from the PROBES catalog [1].

$$v_{h\rm rms}(1) \le \frac{v'_{h\rm rms}(1)}{f}, \tag{7}$$

where $f = 1$ if dark matter is collisional, or

$$f \approx \left(\frac{\rho_{ch}}{\rho_B}\right)^{1/6} \frac{1}{\sqrt{2 \cdot \ln\left(\rho_{ch}/\rho_B\right)}}, \tag{8}$$

if dark matter is collisionless, *i.e.* has less than one collision per orbit. f is a geometrical factor derived in the Appendix, and is presented in **Figure 2**. ρ_B is the background density. We consider Equation (8) to be approximate because it does not take into account the detailed formation of the galaxy halo, and because the background density ρ_B depends on each galaxy and the redshift of observation, but, for this study, we simply take the extreme case $\rho_B = \Omega_c \rho_{\rm crit}/a^3$ with $a = 1$. Alternatively, for collisionless dark matter the paricle orbits are mostly radial so we may take $f \approx \sqrt{3}$, see (2).

Consider a cored isothermal sphere. Its radius $r_{\rm max}$, where it meets the background density, grows due to the expansion of the universe that reduces ρ_B. If dark matter is cold, the new particles falling into the cored isothermal sphere gravitational potential go through the center of the galaxy producing a cusp as observed in cold dark matter simulations. Often small galaxies are observed to have a core, not a cusp. This is the cold dark matter "core-cusp problem". If dark matter is warm, then the angular momentum of the particles falling into the gravitational potential well has a Maxwell distribution, and the collisionless particles have a distance of closest approach to the center of the galaxy that has a Maxwell distribution that defines the core radius of the galaxy, and obtains the factor f mentioned above and derived in the Appendix. Note that f is of cosmological origin,

i.e. it depends on $v_{hrms}(1)$. Note that the core radius r_c, or core density ρ_{ch}, distinguishes cold from warm dark matter. For cold dark matter, $r_c \to 0$ and $\rho_{ch} \to \infty$.

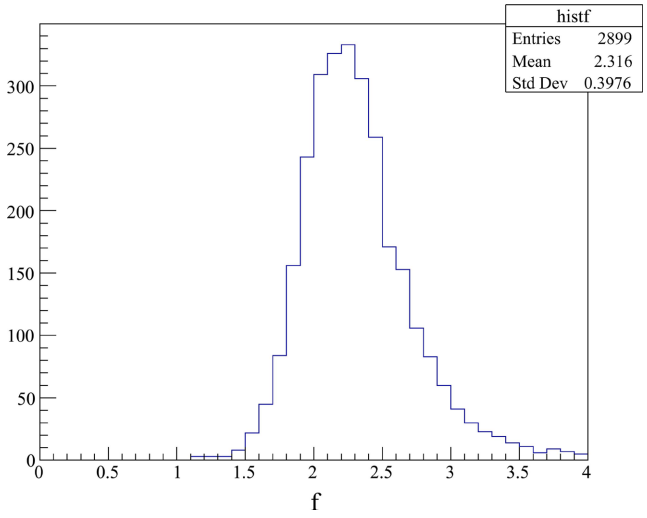

Figure 2. Geometrical correction factor f for collisionless warm dark matter, for $\rho_B = \Omega_c \rho_{\text{crit}} / a^3$ with $a = 1$.

In Equation (7) the equal sign applies if there is no dark matter relaxation or rotation. Rotation of the dark matter halo can only increase the observed $v'_{hrms}(1)$, see [4]. Also relaxation can only increase the observed $v'_{hrms}(1)$, else the phase space density (proportional to $v'_{hrms}(1)^{-3}$) increases. We hope to extract $v_{hrms}(1)$ from the lower bounds of the histograms of $v'_{hrms}(1)/f$.

3. Data

The data is obtained from the PROBES catalog file https://zenodo.org/api/records/10456320/files-archive [1]. This file contains three coma-separated-values files *main_table.csv*, *model_fits.csv* and *structural_parameters.csv*. The file *main_table.csv* contains general information for 3163 galaxies. The file *model_fits.csv* contains the fit parameters to the galaxy rotation curves of 3161 spiral galaxies. To obtain the fit quality parameter *AutoProf_flags* and the distances to the galaxies we need to match galaxies in *main_table.csv* and *model_fits.csv*. This leaves 2899 galaxies. The corresponding histograms below are labeled "histf". Two functional forms for $V(r)$ are fitted:

$$V_{\tanh}(r) = V_{\text{sys}} + V_{\max} \tanh\left((r - r_0)/r_t\right), \tag{9}$$

$$V_{\text{C97}}(r) = V_{\text{sys}} + V_{\max} \frac{\left(1 + r_t/(r - r_0)\right)^{\beta}}{\left(1 + \left(r_t/(r - r_0)\right)^{\gamma}\right)^{1/\gamma}}. \tag{10}$$

The file *structural_parameters.csv* contains detailed parameters of 1675 galaxies obtained from multi-band photometry and spectroscopy. The corresponding his-

tograms below are labeled "histp". The rotation curves are obtained from Hα long-slit spectra and aperture synthesis HI (21 cm) velocity maps. If both fit parameters and photometry data are desired, the corresponding match leaves 579 galaxies. The corresponding histograms below are labeled "histm". These numbers are needed to understand the statistics of the histograms. The PROBES catalog includes data from multiple data sets [6]-[14].

4. Studies

A summary of results $v'_{h\mathrm{rms}}(1)$ and tests is presented in **Figure 3**. In the end we still need to extract the lower bound of these histograms to obtain a measurement of $v_{h\mathrm{rms}}(1)$ with $f=1$, corresponding to collisional dark matter. The first two histograms of **Figure 3** show results with full statistics for the *tanh* and *C*97 fits, respectively. These fits require a match of galaxies between the files *main_table.csv* and *model_fits.csv*, in order to be able to require the *AutoProf_flags* confirmation of a good fit, and to convert r_t of the fits from arcsec to kpc with the distance to each galaxy. For these first two histograms we take $f_M \approx 0.85$ since the information to calculate f_M is not yet available. The third histogram in **Figure 3** is obtained after matching galaxies in all three files *main_table.csv*, *model_fits.csv* and *structural_parameters.csv*.

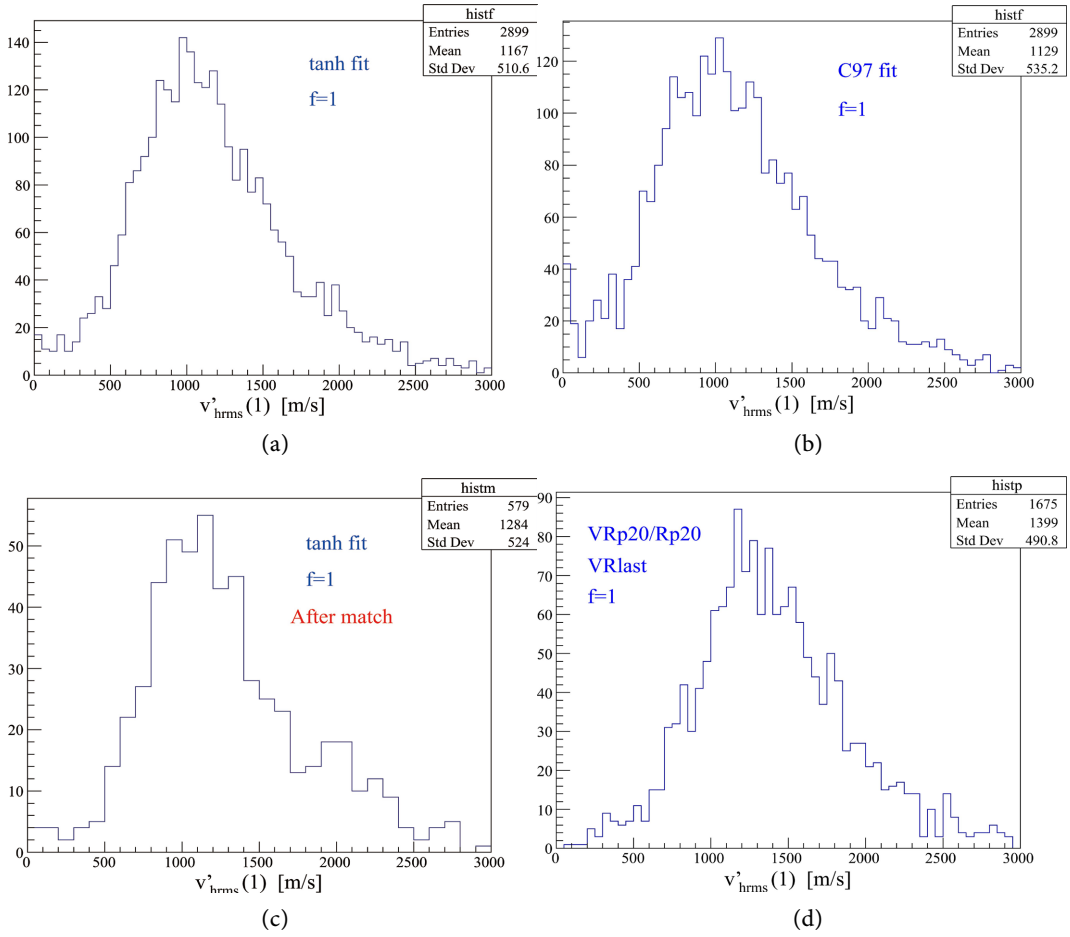

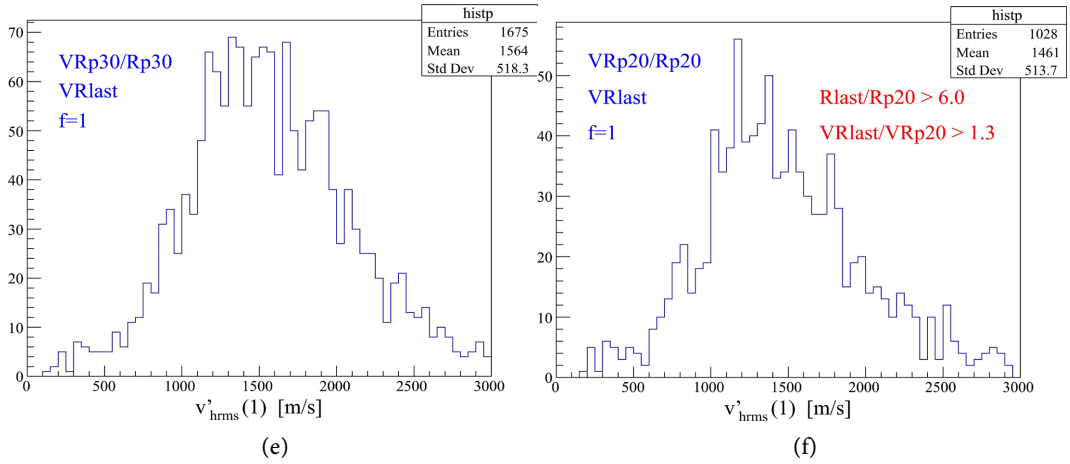

Figure 3. Histograms of $v'_{hrms}(1)$ for collisional dark matter. $f=1$. The histograms are described in the labels and in the main text.

As a cross-check, we present results without using the fits. In this case we take $V_{max} \approx VRlast$ and $V(r_{min})/r_{min} \approx VRp20/Rp20$, where $Rp20$ is the radius enclosing 20% of the stellar light. Also shown is the case for $Rp30$, and the case for $Rp20$ with additional quality cuts.

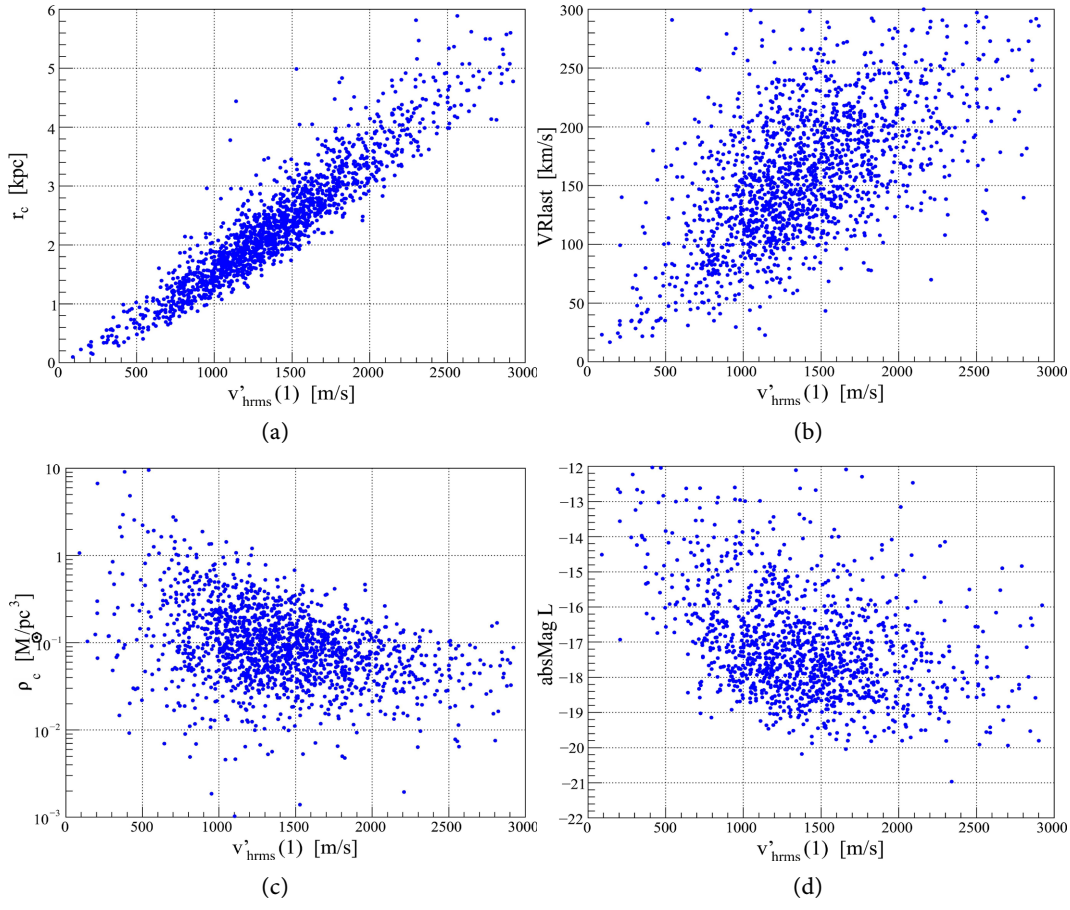

Figure 4. Distributions of $v'_{hrms}(1)$ for collisional dark matter. $f=1$.

Distributions of $v'_{hrms}(1)$ as a function of core radius r_c, the flat rotation velocity V_{max}, the core density ρ_{ch}, and the absolute magnitude L, for the case $f=1$ of collisional dark matter, are presented in **Figure 4**.

Corresponding histograms and distributions of $v'_{hrms}(1)/f$ are presented in **Figure 5** and **Figure 6** with f of (8) for collisionless dark matter.

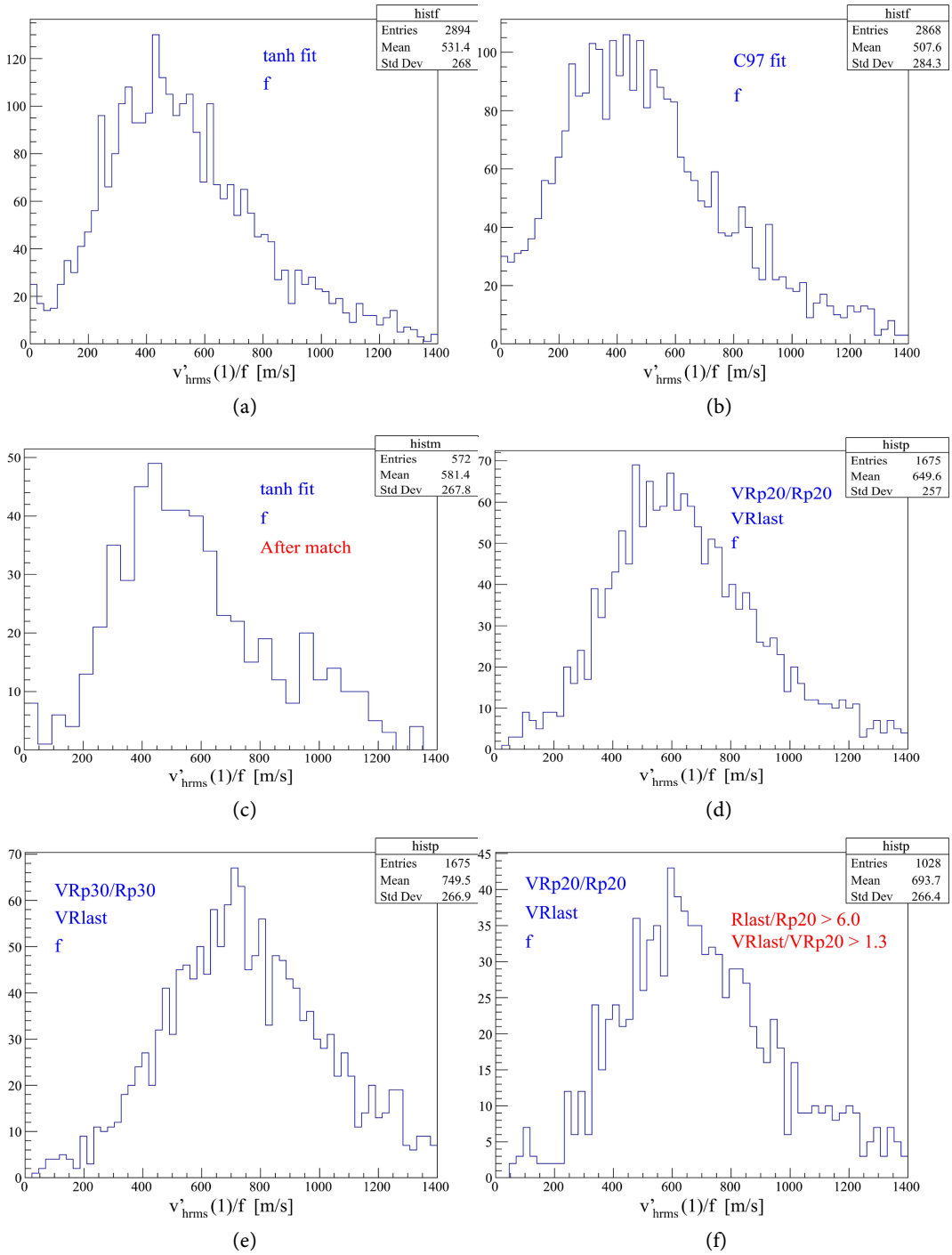

Figure 5. Histograms of $v'_{hrms}(1)/f$ for collisionless dark matter. f from (8). The histograms are described in the labels and in the main text.

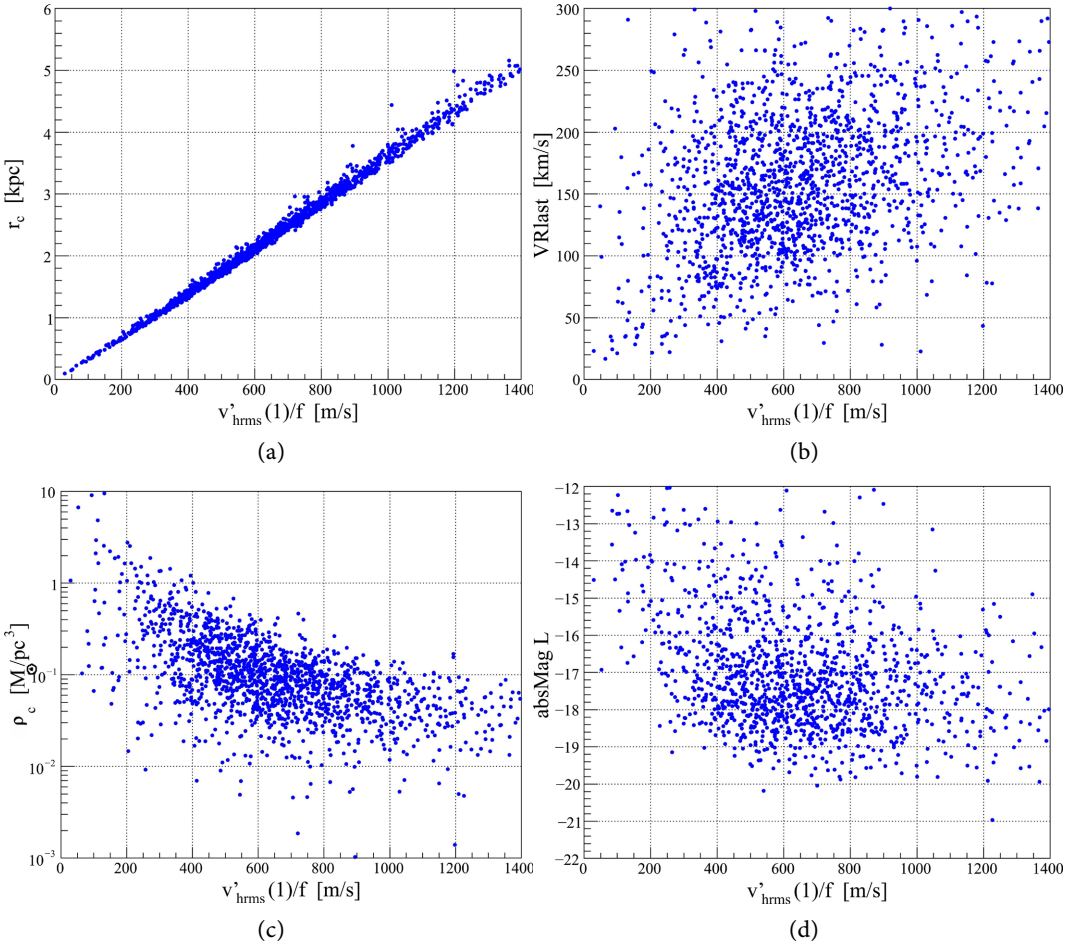

Figure 6. Distributions of $v'_{hrms}(1)/f$ for collisionless dark matter. f from (8). Note that, from the equations in Section 1, $v'_{hrms}(1)/f$ is proportional to r_c up to a logarithmic term.

A careful comparison of collisional and collisionless histograms and distributions shows that the correction f increases their relative widths, indicating that the data have some preference for collisional dark matter.

To test whether the lower bounds of these distributions are of cosmological origin, we present in **Figure 7** extreme cases of low and high absolute luminosity L, stellar mass M_*, and dynamical mass M_{dyn}. In **Figure 8** we present the distributions for several galaxy morphologies. We observe no significant dependence on L, M_*, M_{dyn}, or morphology, suggesting that $v_{hrms}(1)$ is indeed of cosmological origin.

Two complementary graphs are presented in **Figure 9** and **Figure 10**.

5. Discussion

We try to extract $v_{hrms}(1)$, for the case $f=1$, from the distribution of the observed $v'_{hrms}(1)$ in the first histogram of **Figure 3**. If there were no dark matter relaxation or dark matter halo rotation, then the distribution of $v'_{hrms}(1)$ would have a width determined by observational uncertainties. Relaxation and rotation

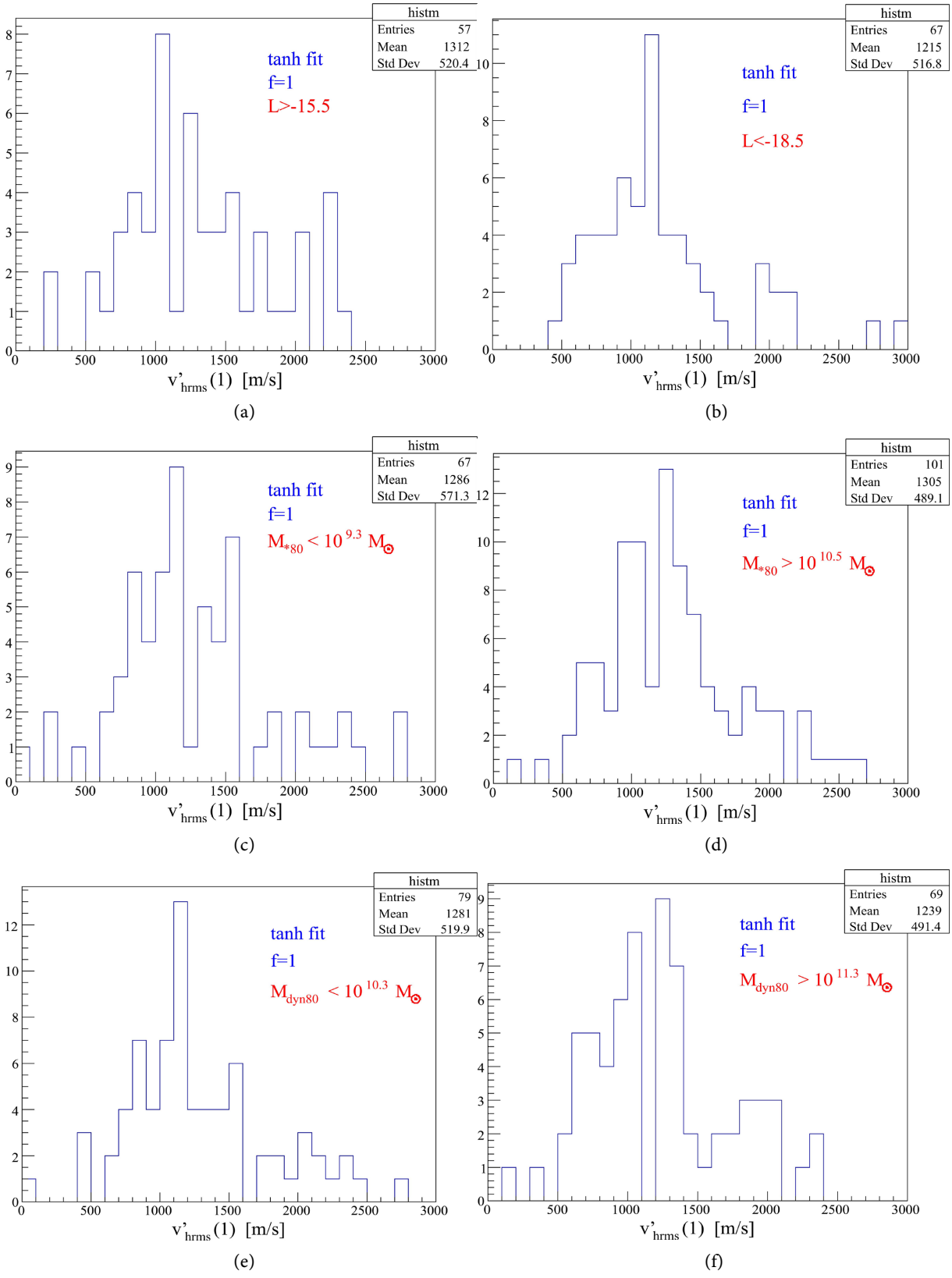

Figure 7. Histograms of $v'_{hrms}(1)$ are shown for extreme low and high absolute luminosities L, stellar mass M_* and dynamical mass M_{dyn} (within the radius containing 80% of the dynamical mass).

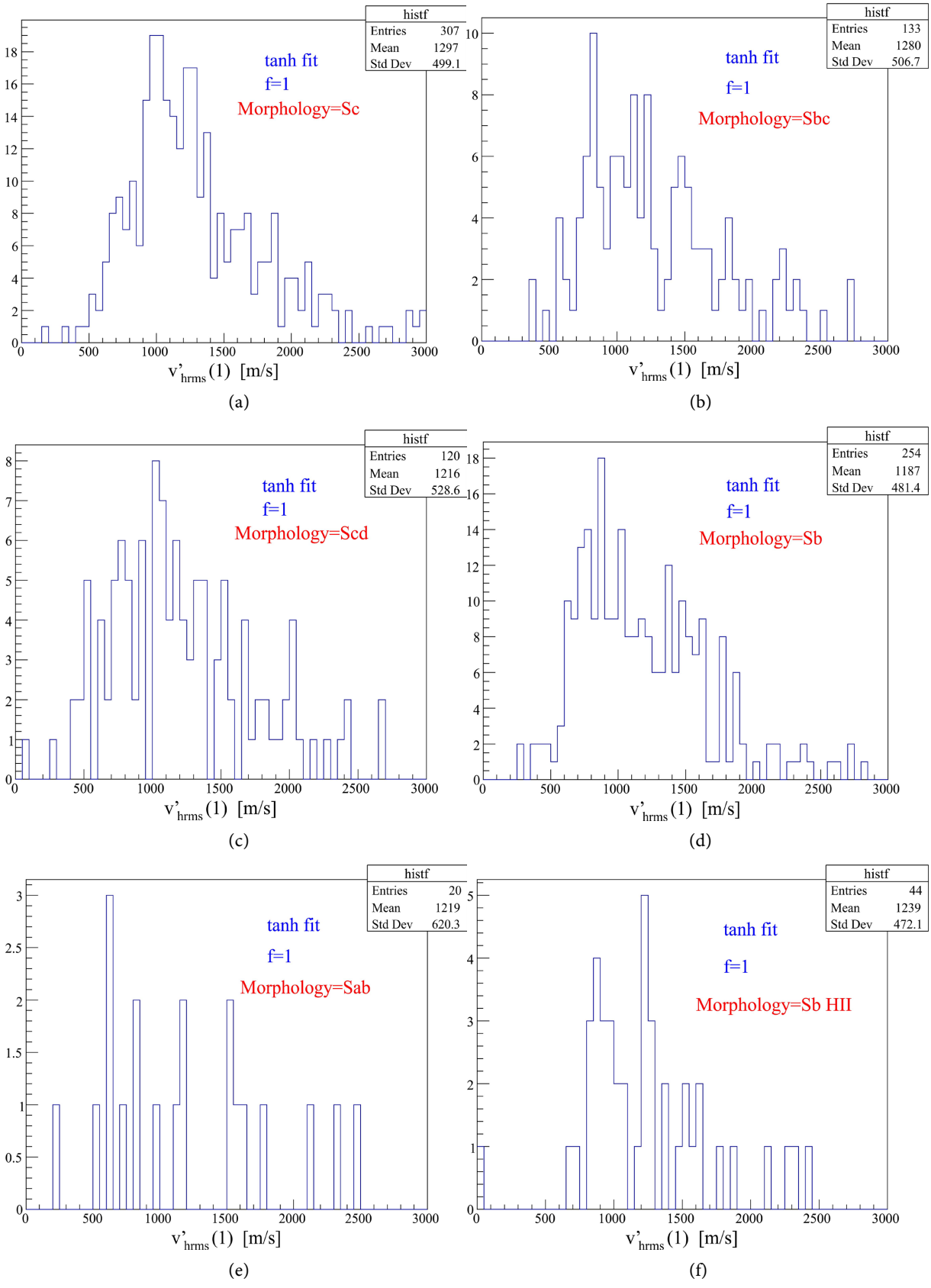

Figure 8. Histograms of $v'_{hrms}(1)$ are shown for several galaxy morphologies.

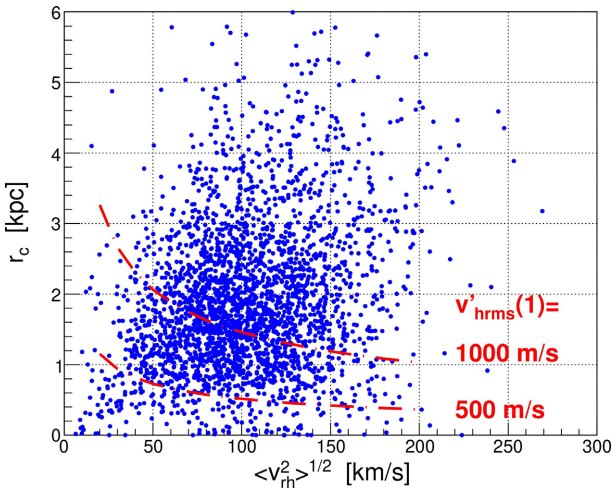

Figure 9. The lower bound for $v'_{hrms}(1)$ is illustrated in 2-dimensions. This graph shows the difficulty of defining the lower bound of $v'_{hrms}(1)$.

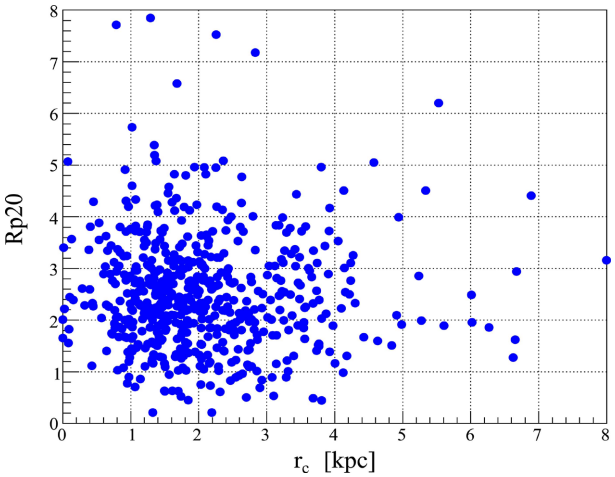

Figure 10. It is interesting to note that, on average, less than 20% of the star light comes from within the core radius r_c.

increase the observed $v'_{hrms}(1)$ by varying amounts for each galaxy. The result is an asymmetrical distribution. Indeed, the distribution has a mean 1030 m/s, and left and right standard deviations 530 m/s and 690 m/s (at points where the histogram is reduced by a factor 1/e).

We are able to reproduce the observed distribution of $v'_{hrms}(1)$ assuming a Gaussian with mean 700 m/s and standard deviation 275 m/s plus a shift to the right, due to relaxation and rotation, with an exponential distribution with mean 560 m/s, see top left histogram of Figure 11. Therefore for collisional dark matter we estimate

$$v_{hrms}(1) = 700 \pm 165 \text{ m/s} \quad \text{for} \quad f = 1, \tag{11}$$

where the uncertainty is estimated as $(1030-700)/2$. To check that the width of the Gaussian distribution is reasonable, see Table 1. The corresponding estimate

for collisionless dark matter is

$$v_{hrms}(1) \approx 280 \pm 95 \text{ m/s} \quad \text{for} \quad f \quad \text{from (8)}, \tag{12}$$

see top right histogram of Figure 11. Equation (12) is approximate because (8) is approximate, and depends on the background density.

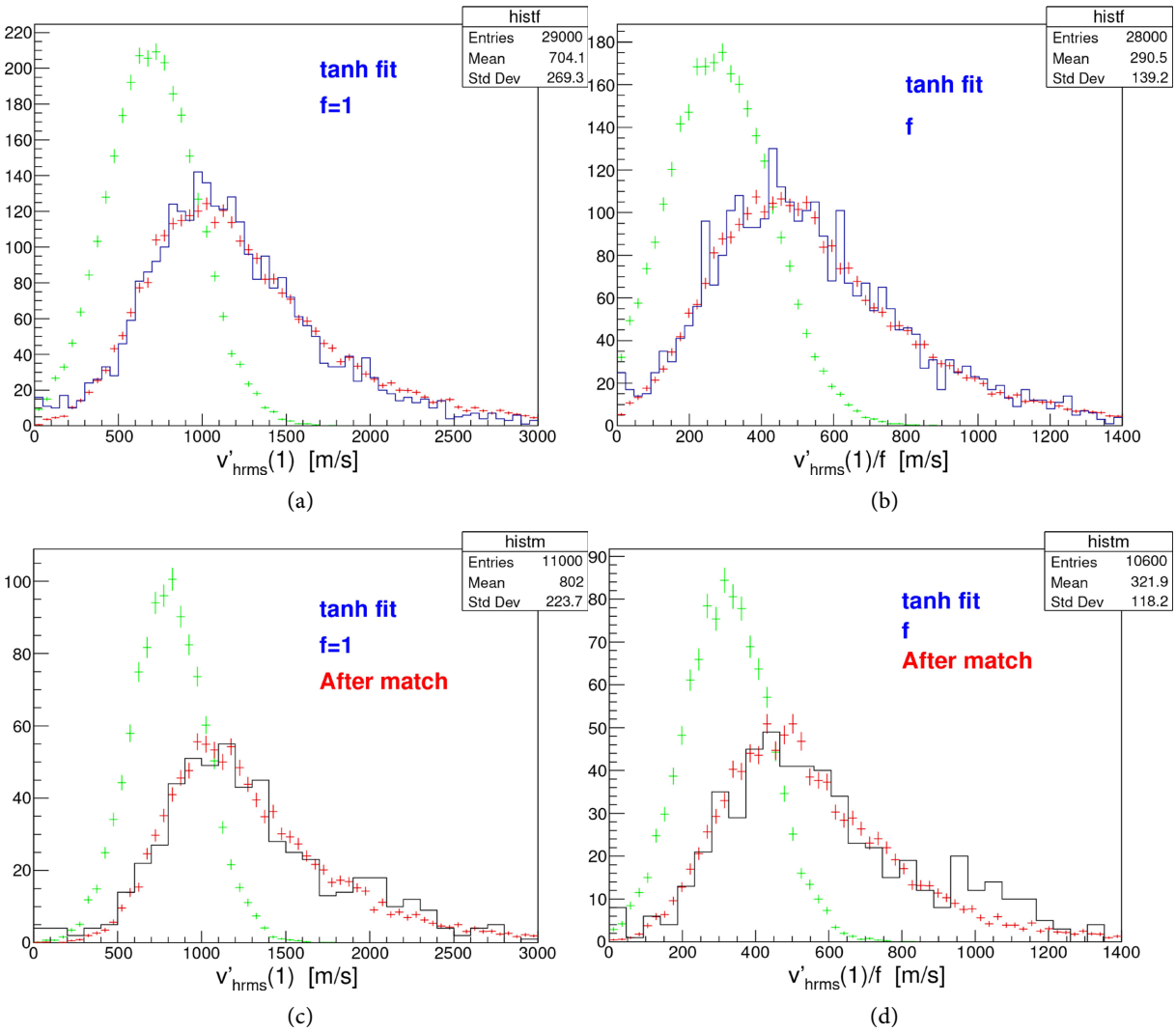

Figure 11. Top-left: Histogram of $v'_{hrms}(1)$ for the *tanh* fit and collisional dark matter with $f = 1$ (as in the first histogram of Figure 3; black), Gaussian with mean 700 m/s and width 275 m/s (green), and same Gaussian plus an exponential distribution to the right, representing relaxation and rotation, with mean 560 m/s (red). Top-right: Same for collisionless dark matter with f from (8). The parameters are Gaussian 280 ± 150 m/s (green), plus exponential distribution to the right with mean 280 m/s (red). Bottom-left: Same for collisional dark matter with $f = 1$ after match. The parameters are Gaussian 800 ± 225 m/s (green), plus exponential distribution to the right with mean 520 m/s (red). Bottom-right: Same for collisionless dark matter with f from (8) after match. The parameters are Gaussian 320 ± 120 m/s (green), plus exponential distribution to the right with mean 240 m/s (red).

As a cross-check, we extract the results from the matched histograms that have a relative width smaller than the corresponding un-matched histograms. We obtain

Table 1. Comparison of galaxy parameters in the PROBES file *structural_parameters.csv* with parameters in [4] plus [5]. $v'_{hrms}(1)$ is calculated with $f=1$ and with the correction f_M. The root-mean-square of the statistical uncertainties of $v'_{hrms}(1)$ in [4] plus [5] is 137 m/s (from the next-to-last column). The root-mean-square difference of $\Delta v'_{hrms}(1)$ between PROBES and [4] plus [5] is 281 m/s (from the last column).

	PROBES				[4] and [5]		Difference
Galaxy	VRlast	ρ_{ch}	$v'_{hrms}(1)$	$\sqrt{2\langle v_{rh}^2\rangle}$	ρ_{ch}	$v'_{hrms}(1)$	$\Delta v'_{hrms}(1)$
	[km/s]	[$M_\odot/pc^3$]	[m/s]	[km/s]	[$M_\odot/pc^3$]	[m/s]	[m/s]
NGC0100	86.6	0.071	802	86	0.0271	1120 ± 160	−318
NGC2366	51.2	0.030	632	50	0.0337	616 ± 44	16
NGC3972	133.5	0.071	1159	118	0.0708	1080 ± 120	79
NGC4183	110.4	0.052	1096	101	0.0522	1010 ± 80	86
NGC4559	119.4	0.033	1270	129	0.0259	1070 ± 50	200
NGC6503	111.3	0.317	615	119	0.1866	750 ± 90	−135
UGC01230	68.5	0.023	889	97	0.0418	1070 ± 130	−181
UGC01281	64.1	0.026	845	56	0.0233	770 ± 100	75
UGC04499	79.7	0.082	714	65	0.0291	780 ± 100	−66
UGC05005	206.2	0.026	2731	87	0.0076	1740 ± 250	991
UGC05750	77.8	0.005	1757	71	0.0065	1450 ± 270	307
UGC06399	88.2	0.038	1006	78	0.0346	910 ± 120	96
UGC06446	83.5	0.106	688	71	0.0811	610 ± 50	78
UGC06667	87.3	0.033	1042	76	0.0389	840 ± 70	202
UGC06917	103.7	0.039	1129	95	0.0354	1040 ± 150	89
UGC07125	67.4	0.010	1179	55	0.0083	1000 ± 130	179
UGC07608	41.2	0.009	740	61	0.0388	690 ± 170	50
UGC10310	47.4	0.049	482	61	0.0405	650 ± 130	−168

$$v_{hrms}(1) = 800 \pm 145 \text{ m/s} \quad \text{for} \quad f=1, \tag{13}$$

$$v_{hrms}(1) \approx 320 \pm 75 \text{ m/s} \quad \text{for} \quad f \quad \text{from (8)}. \tag{14}$$

A simpler procedure that we used in the past (with fewer numbers of galaxies) is to estimate the lower bound of the distributions of $v'_{hrms}(1)$.

The measurements (11) or (12) are in disagreement with limits summarized in **Table 2**. These limits would push the green Gaussians in **Figure 11** to the left. In this case the measured distributions of $v'_{hrms}(1)$ would be due dominantly to relaxation and rotation. To break the degeneracy, we need to complement the measurements (11) or (12) with independent measurements. We also need an understanding of the limits.

6. Comparison with Previous Measurements

Let us compare the $f=1$ case with previous measurements. In [4] we fit the

rotation curves of 11 dwarf galaxies with the result

Table 2. Tightest published lower limits on the "standard thermal relic" [15] warm dark matter mass m_x obtained from different observables (from **Figure 3** of [16]; see citations therein). Also shown are corresponding limits on $a_{h\mathrm{NR}} \equiv v_{h\mathrm{rms}}(1)/c$, $v_{h\mathrm{rms}}(1)$ and k_{fs}, and an approximate redshift of the measurements. The actual dark matter particle mass is model dependent [17].

Observable	m_x	$a_{h\mathrm{NR}}$	$v_{h\mathrm{rms}}(1)$	k_{fs}	Typical z
	[keV]		[m/s]	[Mpc^{-1}]	
Milky Way satellites	$\gtrsim 10$	$\lesssim 3.3\times10^{-8}$	$\lesssim 10$	$\gtrsim 71$	0
Strong lensing	$\gtrsim 6.0$	$\lesssim 5.7\times10^{-8}$	$\lesssim 17$	$\gtrsim 40$	0 to 1
Lyman-α forest	$\gtrsim 5.2$	$\lesssim 6.7\times10^{-8}$	$\lesssim 20$	$\gtrsim 34$	6
Galaxy UV luminosity	$\gtrsim 3.2$	$\lesssim 1.2\times10^{-7}$	$\lesssim 35$	$\gtrsim 20$	6 to 8
γ ray burst	$\gtrsim 1.8$	$\lesssim 2.2\times10^{-7}$	$\lesssim 66$	$\gtrsim 11$	4 to 8

$$v_{h\mathrm{rms}}(1) = 406 \pm 69 \text{ m/s}. \tag{15}$$

The rotation curves where obtained by the "Local Irregulars That Trace Luminosity Extremes—The HI Nearby Galaxy Survey" (LITTLE THINGS) collaboration [18]. In [17] we fit the rotation curves of 36 co-added dwarf disk galaxies, obtained from [19], with the result

$$v_{h\mathrm{rms}}(1) = 515 \pm 15(\mathrm{stat}) \text{ m/s}. \tag{16}$$

These measurements are in agreement with lower bounds of distributions of $v'_{h\mathrm{rms}}(1)$ with dwarf [4] and spiral [5] galaxy rotation curves, or density runs of elliptical galaxies [20]. Since the absolute luminosity of these galaxies span 4 orders of magnitude, and the baryon central densities span 6 orders of magnitude, we interpret these lower bounds to be of cosmological origin, *i.e.* $v_{h\mathrm{rms}}(1)$.

The warm dark matter comoving thermal velocity $v_{h\mathrm{rms}}(1)$ causes a cut-off of the comoving cold dark matter linear density power spectrum by a factor of the form $\tau^2(k) = \exp\left(-k^2/k_{\mathrm{fs}}^2\right)$ due to free-streaming (assuming the dark matter particles have a Maxwell distribution of velocities). The comoving cut-off wavevector k_{fs} is related to $v_{h\mathrm{rms}}(1)$ by [21] [22]

$$k_{\mathrm{fs}}(t_{\mathrm{gal}}) = 1.41 \text{ Mpc}^{-1} \frac{493 \text{ m/s}}{v_{h\mathrm{rms}}(1)} = 0.88 \sqrt{\frac{4\pi G \Omega_m \rho_{\mathrm{crit}} a_{\mathrm{eq}}}{v_{h\mathrm{rms}}^2(1)}}. \tag{17}$$

This equation is approximately valid for collisionless or collisional dark matter [22]. t_{gal} is a time prior to the formation of first galaxies and the corresponding non-linear re-generation of perturbations. The independent measurements of $v_{h\mathrm{rms}}(1)$ and $k_{\mathrm{fs}}(t_{\mathrm{gal}})$ cross-check each other. Limits in the literature are often expressed as limits on the "standard thermal relic mass" m_x. The relation between m_x and k_{fs} is often given by Equations (6) and (7) of [15].

From galaxy stellar mass and ultra-violet luminosity distributions in a wide redshift range we obtain [23]

$$k_{\mathrm{fs}} = 2.0^{+0.8}_{-0.5}\ \mathrm{Mpc}^{-1} \quad \text{or} \quad v_{h\mathrm{rms}}(1) = 348^{+115}_{-100}\ \mathrm{m/s}. \tag{18}$$

The observed re-ionization of the universe requires a delayed galaxy formation compared to the ΛCDM scenario. This delay requires $m_x = 0.51^{+0.22}_{-0.12}$ keV [24], or $k_{\mathrm{fs}} \approx 2 \pm 1\ \mathrm{Mpc}^{-1}$ [25], or $m_x = 1.3^{+0.3}_{-0.7}$ keV [26], or $m_x = 0.66^{+0.07}_{-0.08}$ keV [26].

All of these measurements are in agreement with each other within $\approx 1.5\sigma$, but in disagreement with the limits summarized in **Table 2**. These disagreements may have been partially understood in [27].

7. A Comment on Warm Dark Matter Limits

The "warmness" of dark matter is defined by two related parameters: the comoving root-mean-square thermal velocity $v_{h\mathrm{rms}}(1)$, and the linear density power spectrum comoving cut-off wavevector k_{fs} due to warm dark matter free-streaming. Studies of galaxy cores obtain *measurements* of $v_{h\mathrm{rms}}(1)$. Studies of dwarf galaxy number densities or stellar masses obtain *limits* on k_{fs}. The relation (17) between $v_{h\mathrm{rms}}(1)$ and k_{fs} seems reliable [21] [22]. Both measurements and limits have issues. In this section we briefly present issues with the limits.

The limits on k_{fs} are often expressed in terms of a lower limit to the "standard therml relic mass" defined by equations (6) and (7) in [15], see **Table 2**. To obtain reliable limits at least the following four issues need to be fully understood and included in the analysis:

1) Most limits are based on observations at low redshift when non-linear regeneration of the power spectrum is large or even dominant [28]-[31].

2) During galaxy formation and hierarchical evolution, small galaxies loose mass to larger galaxies, so "stripped down" galaxies need to be included in the analysis [27] [32].

3) Consider a linear density perturbation on the mass scale $M_{\mathrm{PS}} = \frac{4}{3}\pi r^3 \bar{\rho} = \frac{4}{3}\pi (1.555/k)^3 \bar{\rho}$. Choose $k < k_{\mathrm{fs}}$ so dark matter free-streaming can be neglected. The Press-Schechter formalism assumes that the observed galaxies have a peak linear relative over-density filtered on the scale M_{PS} equal to the critical value 1.686 (corresponding to spherical collapse in the linear approximation, that has already broken down). If the peak is less than 1.686 the halo on this mass scale has not yet collapsed. If the peak is greater than 1.686 then the halo collapsed earlier and belongs to a larger mass M_{PS}. This assumption is an approximation: it does not apply to lower density regions. Density perturbations of comoving radius r have a distribution of relative overdensities $\delta(a)$ (assumed Gaussian in the Press-Schechter formalism), so that galaxy halos with a given M_{PS} are formed with a distribution of times that extend to the present and future, and distributions of flat orbital velocities and stellar masses that extend to zero in less dense regions of the universe. In conclusion, observations of dwarf galaxy stellar masses or number densities can not place a limit on k_{fs} unless the time of formation of the galaxy halos is well known and included in the analysis. In other words, the initial linear perturbation is described by three parameters, *i.e.*

k, $\delta(a)$ and the initial background density δ_B, while the observations are often based on a single parameter, so there is no one-to-one relation between these observations and k or k_{fs}. The relation between multiple observations and k_{fs} is complex.

4) Observed galaxies are biased to regions of high background density. Accounting for this bias weakens the limits based on dwarf galaxy counts in overdense regions (because of the reduced expansion of overdense regions that form the sheets, filaments and nodes where most galaxies reside).

8. A Comment on Collisional Dark Matter

Consider a dark matter particle falling into a cored isothermal sphere from $r_{\max}$ to r_c. Let σ be the dark matter-dark matter collision cross-section, which we take to be independent of the center of mass energy for non-relativistic dark matter [33]. The cross-section per unit mass corresponding to one collision on average is

$$\frac{\sigma}{m_h} \approx \frac{2\pi G r_c}{\left\langle v_{rh}^2 \right\rangle} = \frac{1}{r_c \rho_{ch}}. \tag{19}$$

The same result is obtained for traversing the radius r_c of the core with 1 collision on average. For $r_c = 1$ kpc and $\left\langle v_{rh}^2 \right\rangle^{1/2} = 60$ km/s we obtain $\sigma/m_h = 36$ cm^2/g. The current limit is <0.47 cm^2/g [3]. In conclusion, it seems that as far as the size of the galaxy halo is concerned, we may consider dark matter to be collisionless. This argument favors the collisionless solution (12) over the collisional solution (11). On the other hand, a detailed comparison of **Figure 3** and **Figure 4** with **Figure 5** and **Figure 6** favors the collisional solution.

9. Conclusion

We have measured the dark matter "warmness", *i.e.* the adiabatic invariant $v_{h\mathrm{rms}}(1)$, with nearly 3000 spiral galaxy rotation curves in the PROBES catalog, assuming collisional or collisionless dark matter [1]. Within statistical fluctuations, the results are independent of the absolute luminosity, stellar mass, dynamical mass and galaxy morphology, suggesting that the measured $v_{h\mathrm{rms}}(1)$ is of cosmological origin. The main uncertainty of the measurements is due to the unknown contribution from relaxation and rotation. To lift this degeneracy it is necessary to complement the present measurement with as many independent measurements as possible. Indeed, we find agreements within $\approx 1.5\sigma$ with previous measurements. There is, however, a discrepancy between the measurements and limits summarized in **Table 2** that is not currently understood.

Acknowledgements

The data in this study was obtained from the PROBES catalog [1]. I thank all authors of [1], and in particular Connor Stone for his help along the way. This catalog has inputs from data sets [6]-[14], which in turn have inputs from many as-

tronomers, so a large community of researchers has made this study possible. I thank Karsten Müller for his early interest in this work and for many useful discussions.

Conflicts of Interest

The author declares no conflicts of interest regarding the publication of this paper.

References

[1] Stone, C., Courteau, S., Arora, N., Frosst, M. and Jarrett, T.H. (2022) PROBES. I. A Compendium of Deep Rotation Curves and Matched Multiband Photometry. *The Astrophysical Journal Supplement Series*, **262**, Article 33. https://doi.org/10.3847/1538-4365/ac83ad

[2] Hoeneisen, B. (2023) Understanding the Formation of Galaxies with Warm Dark Matter. *Journal of Modern Physics*, **14**, 1741-1754. https://doi.org/10.4236/jmp.2023.1413103

[3] Navas, S., *et al.* (2024) The Review of Particle Physics. *Physical Review D*, **110**, Article ID: 030001.

[4] Hoeneisen, B. (2022) Measurement of the Dark Matter Velocity Dispersion with Dwarf Galaxy Rotation Curves. *International Journal of Astronomy and Astrophysics*, **12**, 363-381. https://doi.org/10.4236/ijaa.2022.124021

[5] Hoeneisen, B. (2019) The Adiabatic Invariant of Dark Matter in Spiral Galaxies. *International Journal of Astronomy and Astrophysics*, **9**, 355-367.

[6] Mathewson, D.S., Ford, V.L. and Buchhorn, M. (1992) A Southern Sky Survey of the Peculiar Velocities of 1355 Spiral Galaxies. *The Astrophysical Journal Supplement Series*, **81**, Article 413. https://doi.org/10.1086/191700

[7] Mathewson, D.S. and Ford, V.L. (1996) Parameters of 2447 Southern Spiral Galaxies for Use in the Tully-Fisher Relation. *The Astrophysical Journal Supplement Series*, **107**, Article 97. https://doi.org/10.1086/192356

[8] Courteau, S. (1996) Deep R-Band Photometry for Northern Spiral Galaxies. *The Astrophysical Journal Supplement Series*, **103**, Article 363. https://doi.org/10.1086/192281

[9] Courteau, S. (1997) Optical Rotation Curves and Linewidths for Tully-Fisher Applications. *The Astronomical Journal*, **114**, Article 2402. https://doi.org/10.1086/118656

[10] Dale, D.A., Giovanelli, R., Haynes, M.P., Campusano, L.E. and Hardy, E. (1999) Seeking the Local Convergence Depth. V. Tully-Fisher Peculiar Velocities for 52 Abell Clusters. *The Astronomical Journal*, **118**, 1489-1505. https://doi.org/10.1086/301048

[11] Courteau, S., Willick, J.A., Strauss, M.A., Schlegel, D. and Postman, M. (2000) Shellflow. I. The Convergence of the Velocity Field at 6000 Kilometers Per Second. *The Astrophysical Journal*, **544**, 636-640. https://doi.org/10.1086/317234

[12] Lelli, F., McGaugh, S.S. and Schombert, J.M. (2016) Sparc: Mass Models for 175 Disk Galaxies with Spitzer Photometry and Accurate Rotation Curves. *The Astronomical Journal*, **152**, Article 157. https://doi.org/10.3847/0004-6256/152/6/157

[13] Ouellette, N.N.-Q., Courteau, S., Holtzman, J.A., Dutton, A.A., Cappellari, M., Dalcanton, J.J., *et al.* (2017) The Spectroscopy and H-Band Imaging of Virgo Cluster Galaxies (SHIVir) Survey: Scaling Relations and the Stellar-to-Total Mass Relation. *The Astrophysical Journal*, **843**, Article 74. https://doi.org/10.3847/1538-4357/aa74b1

[14] Ouellette, N.N., Courteau, S., Holtzman, J.A., McDonald, M., Cappellari, M., Roediger, J.C., *et al.* (2022) The Spectroscopy and *H*-Band Imaging of Virgo Cluster Galaxies (SHIVir) Survey: Data Catalogue and Kinematic Profiles. *Monthly Notices of the Royal Astronomical Society*, **514**, 2356-2375. https://doi.org/10.1093/mnras/stac1347

[15] Viel, M., Lesgourgues, J., Haehnelt, M.G., Matarrese, S. and Riotto, A. (2005) Constraining Warm Dark Matter Candidates Including Sterile Neutrinos and Light Gravitinos with WMAP and the Lyman-α forest. *Physical Review D*, **71**, Article ID: 063534. https://doi.org/10.1103/physrevd.71.063534

[16] Liu, B., Shan, H. and Zhang, J. (2024) New Galaxy UV Luminosity Constraints on Warm Dark Matter from JWST. *The Astrophysical Journal*, **968**, Article 79. https://doi.org/10.3847/1538-4357/ad4ed8

[17] Hoeneisen, B. (2024) Measurements of the Dark Matter Mass, Temperature and Spin. *International Journal of Astronomy and Astrophysics*, **14**, 184-202. https://doi.org/10.4236/ijaa.2024.143012

[18] Oh, S., Hunter, D.A., Brinks, E., Elmegreen, B.G., Schruba, A., Walter, F., *et al.* (2015) High-Resolution Mass Models of Dwarf Galaxies from Little Things. *The Astronomical Journal*, **149**, Article 180. https://doi.org/10.1088/0004-6256/149/6/180

[19] Karukes, E.V. and Salucci, P. (2017) The Universal Rotation Curve of Dwarf Disc Galaxies. *Monthly Notices of the Royal Astronomical Society*, **465**, 4703-4722. https://doi.org/10.1093/mnras/stw3055

[20] Hoeneisen, B. (2024) Understanding Elliptical Galaxies with Warm Dark Matter. *Physics of the Dark Universe*, **46**, Article 101643. https://doi.org/10.1016/j.dark.2024.101643

[21] Boyanovsky, D., de Vega, H.J. and Sanchez, N.G. (2008) Dark Matter Transfer Function: Free Streaming, Particle Statistics, and Memory of Gravitational Clustering. *Physical Review D*, **78**, Article ID: 063546. https://doi.org/10.1103/physrevd.78.063546

[22] Hoeneisen, B. (2025) The Warm Dark Matter Plus Baryon Linear Power Spectrum. *International Journal of Astronomy and Astrophysics*, **15**, 264-281. https://doi.org/10.4236/ijaa.2025.153017

[23] Hoeneisen, B. (2024) Are James Webb Space Telescope Observations Consistent with Warm Dark Matter? *International Journal of Astronomy and Astrophysics*, **14**, 45-60. https://doi.org/10.4236/ijaa.2024.141003

[24] Lin, H., Gong, Y., Yue, B. and Chen, X. (2023) Implications of the Stellar Mass Density of High-Z Massive Galaxies from JWST on Warm Dark Matter. *Research in Astronomy and Astrophysics*, **24**, Article 015009. https://doi.org/10.1088/1674-4527/ad0864

[25] Hoeneisen, B. (2022) Measurement of the Dark Matter Velocity Dispersion with Galaxy Stellar Masses, UV Luminosities, and Reionization. *International Journal of Astronomy and Astrophysics*, **12**, 258-272. https://doi.org/10.4236/ijaa.2022.123015

[26] Lapi, A., Ronconi, T., Boco, L., Shankar, F., Krachmalnicoff, N., Baccigalupi, C., *et al.* (2022) Astroparticle Constraints from Cosmic Reionization and Primordial Galaxy Formation. *Universe*, **8**, Article 476. https://doi.org/10.3390/universe8090476

[27] Hoeneisen, B. (2025) Discrepancies between Limits and Measurements of Warm Dark Matter Properties. *International Journal of Astronomy and Astrophysics*, **15**, 65-79. https://doi.org/10.4236/ijaa.2025.152005

[28] Parimbelli, G., Scelfo, G., Giri, S.K., Schneider, A., Archidiacono, M., Camera, S., *et*

al. (2021) Mixed Dark Matter: Matter Power Spectrum and Halo Mass Function. *Journal of Cosmology and Astroparticle Physics*, **2021**, Article 044. https://doi.org/10.1088/1475-7516/2021/12/044

[29] MacInnis, A., and Sehgal, N. (2024) CMB-HD as a Probe of Dark Matter on Sub-Galactic Scales. arxiv:2405.12220.

[30] Despali, G., Moscardini, L., Nelson, D., Pillepich, A., Springel, V. and Vogelsberger, M. (2025) Introducing the AIDA-TNG Project: Galaxy Formation in Alternative Dark Matter Models. *Astronomy & Astrophysics*, **697**, A213. https://doi.org/10.1051/0004-6361/202553836

[31] Schneider, A., Smith, R.E., Macci'o, A.V. and Moore, B. (2012) Nonlinear Evolution of Cosmological Structures in Warm Dark Matter models. arxiv:1112.0330.

[32] Hoeneisen, B. (2019) Simulations and Measurements of Warm Dark Matter Free-Streaming and Mass. *International Journal of Astronomy and Astrophysics*, **9**, 368-392. https://doi.org/10.4236/ijaa.2019.94026

[33] Hoeneisen, B. (2021) Adding Dark Matter to the Standard Model. *International Journal of Astronomy and Astrophysics*, **11**, 59-72. https://doi.org/10.4236/ijaa.2021.111004

Appendix

Core radius

Consider a cored isothermal sphere with core density ρ_c and core radius r_c in a background of density $\rho_B(t)$. The halo meets the background density at $r_{\max} = r_c\sqrt{\rho_c/\rho_B(t)}$. As the universe expands, the background density decreases and $r_{\max}$ increases. The new particles being captured by the growing halo have a transverse root-mean-square velocity component $v_T = \left(1/\sqrt{3}\right)v_{h\mathrm{rms}}(1)\left(\rho_B/\left(\Omega_c\rho_{\mathrm{crit}}\right)\right)^{1/3}$. We assume collisionless dark matter. Conservation of angular momentum tells us that these particles pass the center of the halo at a root-mean-square distance $r_{\min} = r_{\max}v_T\Big/\sqrt{4\left\langle v_{rh}^2\right\rangle\ln\left(r_{\max}/r_c\right)}$. Identifying $r_{\min}$ with r_c, we obtain

$$v_{h\mathrm{rms}}(1) = \frac{v'_{h\mathrm{rms}}(1)}{f}, \tag{20}$$

with

$$f = \left(\frac{\rho_c}{\rho_B}\right)^{1/6}\frac{1}{\sqrt{2\cdot\ln\left(\rho_c/\rho_B\right)}}. \tag{21}$$

Note that, if the core is dominated by warm dark matter and there is no relaxation or halo rotation, $v'_{h\mathrm{rms}}(1)/f$ is of cosmological origin.